Composite Structures xxx (2015) xxx–xxx

Contents lists available at ScienceDirect

Composite Structures

journal homepage: www.elsevier.com/locate/compstruct

A comparative study of continuous beams prestressed with bonded FRP and steel tendons

Tiejiong Lou [a,*], Sergio M.R. Lopes [a], Adelino V. Lopes [b]

[a] CEMUC, Department of Civil Engineering, University of Coimbra, Coimbra 3030-788, Portugal
[b] Department of Civil Engineering, University of Coimbra, Coimbra 3030-788, Portugal

ARTICLE INFO

Article history:
Available online xxxx

Keywords:
Prestressed concrete
Continuous beams
FRP tendons
Finite element analysis

ABSTRACT

This paper presents a numerical investigation of the performance of continuous prestressed concrete beams with bonded fiber reinforced polymer (FRP) and steel tendons. A finite element model has been developed and is validated against the available test data. A numerical test is carried out on two-span continuous bonded prestressed concrete beams. Three types of tendons are considered for a comparative study: aramid FRP (AFRP), carbon FRP (CFRP) and prestressing steel. Various levels of ω_p (reinforcement index of prestressing tendons) are used. The results indicate that, with increasing ω_p, the failure mode of FRP prestressed concrete beams would transit from tendon rupture to concrete crushing while the crushing failure always takes place in steel prestressed concrete beams. Moreover, FRP tendons mobilize significantly different behavior regarding the crack pattern, deformation characteristics and neutral axis depth compared to steel tendons. The moment redistribution at ultimate in AFRP prestressed concrete beams is comparable to that in steel prestressed concrete beams while, at a low ω_p level, CFRP tendons register obviously lower redistribution than steel tendons.

1. Introduction

Fiber reinforced polymer (FRP) composites have been widely employed for reinforcing concrete structures instead of traditional steel reinforcement [1–3]. FRP materials offer attractive benefits, including high tensile strength, noncorrosive and nonmagnetic properties, favorable fatigue resistance and low weight [4]. In the field of prestressing systems, FRP tendons are a promising alternative to traditional steel tendons which are susceptible to corrosive damage. One of the primary concerns for practical applications of FRP tendons is related to anchorages [5]. Over past years, many studies have been undertaken regarding the anchorage systems for FRP tendons [6–10]. There are three basic composite materials that may be used for prestressing tendons: glass FRP (GFRP), aramid FRP (AFRP) and carbon FRP (CFRP). GFRP composites are not recommended for bonded tendons because of the poor resistance to alkaline environment and also to creep under sustained loads [11]. AFRP and CFRP composites are both desired for composite tendons and have been widely used for prestressing applications.

FRP tendons possess different material properties compared to steel tendons. FRP composites are brittle in nature, with linear elastic behavior up to rupture. AFRP tendons have usually a much lower modulus of elasticity than steel tendons, while the elastic modulus of CFRP tendons covers a wide range from 80 to 500 MPa [12]. Therefore, the common knowledge established from conventional steel prestressed concrete beams may not be applicable to FRP prestressed concrete beams. Many efforts have been made to understand the behavior of concrete beams prestressed with FRP tendons. Pisani [13] described a numerical study on the flexural behavior of simply supported bonded and unbonded prestressed concrete beams with steel and FRP tendons. Park and Naaman [14] reported the test results regarding the shear behavior of CFRP prestressed concrete simply supported beams. Toutanji and Saafi [15] tested a series of four simply supported concrete beams prestressed AFRP tendons to study the flexural performance of these beams. The tests indicated that the use of combined bonded and unbonded AFRP tendons or of additional nontensioned rebars can improve notably the ductile behavior. Stoll et al. [16] presented the results of a test program performed on two full-scale simply supported high-strength concrete bridge girders prestressed with CFRP tendons. Dolan and Swanson [17] conducted a theoretical and experimental study on the flexural capacity of simply supported beams prestressed with vertically distributed FRP tendons. Kim [18] examined the effect of prestress level on the behavior of simply supported AFRP prestressed concrete beams and also checked the applicability of several design codes and existing predictive equations.

* Corresponding author. Tel.: +351 239797253.
E-mail address: loutiejiong@dec.uc.pt (T. Lou).

http://dx.doi.org/10.1016/j.compstruct.2015.01.009
0263-8223/© 2015 Published by Elsevier Ltd.

Although extensive works have been carried out regarding the behavior of prestressed concrete beams with bonded FRP tendons, most of the past works dealt only with the simply support condition. Few attempts have so far been made to investigate the behavior of continuous FRP prestressed beams. The authors [19–21] have recently conducted a set of theoretical studies to evaluate the response of continuous external FRP tendon systems, with particular emphasis placed on the redistribution of moments. Because of the bond effects and nonexistence of second-order effects, internal bonded tendon systems would behave differently from external tendon systems.

This paper describes a numerical study that is conducted to reveal the flexural behavior of two-span continuous concrete beams prestressed with internal bonded FRP and steel tendons. A numerical model for geometric and material nonlinear analysis of bonded prestressed concrete continuous beams has been developed. The proposed model is verified with the experimental results available in the literature. A comparative study on the performance of AFRP, CFRP and steel prestressed concrete continuous beams is carried out by using the proposed model. Various amounts of prestressing tendons are used for the numerical evaluation. Some findings are concluded.

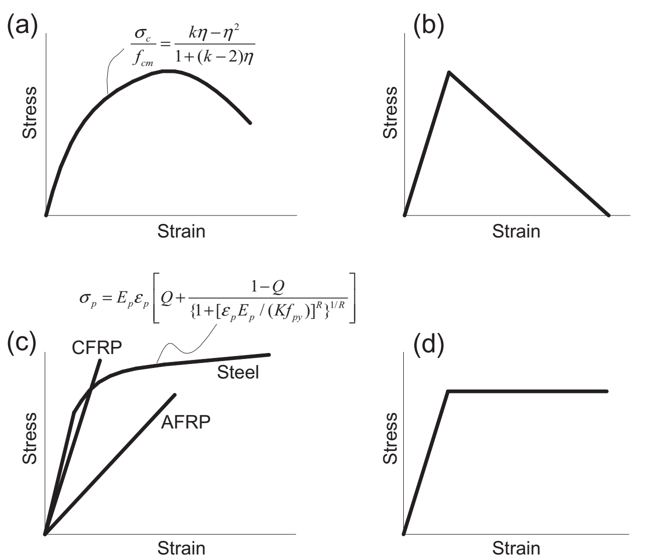

Fig. 1. Stress–strain curves of materials. (a) Concrete in compression; (b) concrete in tension; (c) prestressing tendons; (d) nonprestressed steel.

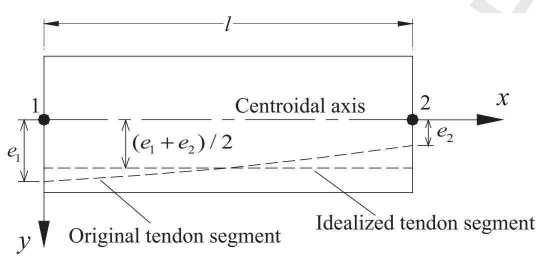

Fig. 2. Beam element with idealized tendon segment.

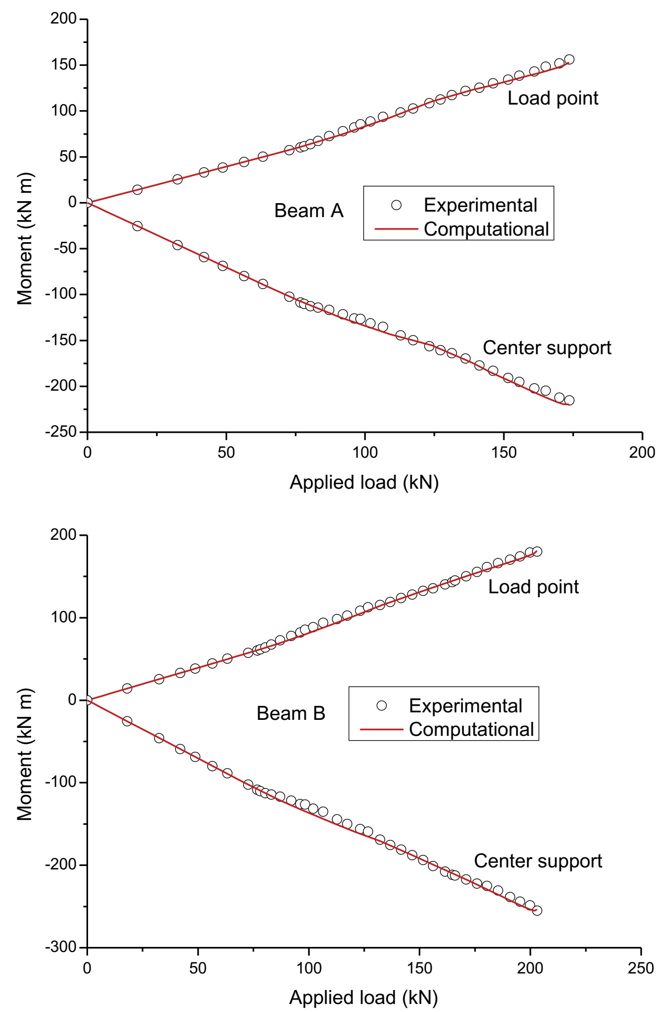

Fig. 4. Comparison between experimental and computational results regarding the load-moment response for the test beams.

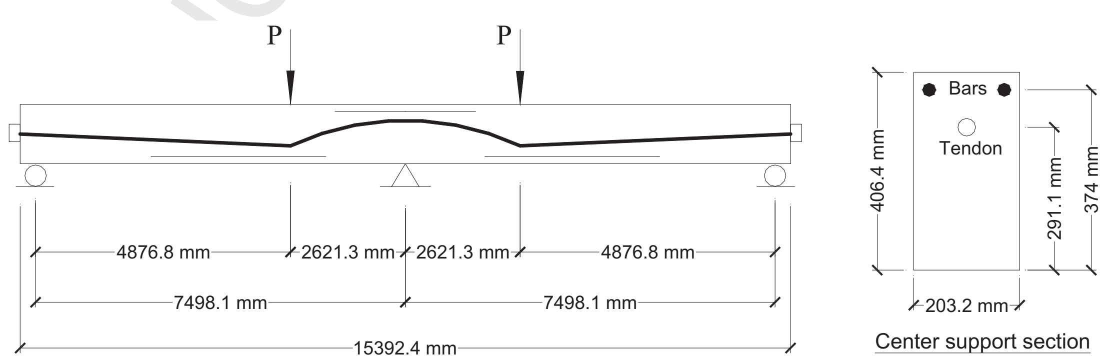

Fig. 3. Test beams by Lin [26].

Please cite this article in press as: Lou T et al. A comparative study of continuous beams prestressed with bonded FRP and steel tendons. Compos Struct (2015), http://dx.doi.org/10.1016/j.compstruct.2015.01.009

2. Nonlinear model

2.1. Stress–strain curves of materials

A stress–strain equation for concrete in uniaxial compression is recommended in Eurocode 2 [22] for structural analysis of concrete members. The stress–strain curve is shown in Fig. 1(a), where $\eta = \varepsilon_c/\varepsilon_{c0}$; σ_c and ε_c are the concrete stress and strain, respectively; k is a coefficient depending on the concrete modulus of elasticity E_c, strain at peak stress ε_{c0} and mean compressive strength f_{cm}. The concrete is assumed to be crushed when its strain reaches the specified ultimate compressive strain ε_u.

The concrete in tension is assumed to be linear elastic prior to cracking and linear strain-softening after cracking, as shown in Fig. 1(b). The concrete tensile strain at the end of strain-softening is taken as 10 ε_{cr}, where ε_{cr} is the cracking strain.

The stress–strain equation for prestressing steel proposed by Menegotto and Pinto [23] is used in this study. The stress–strain curve is shown in Fig. 1(c), where σ_p and ε_p are the tendon stress and strain, respectively; E_p is the tendon modulus of elasticity; f_{py} is the yield stress of prestressing steel; and K, Q and R are empirical parameters which can be determined by experimental data.

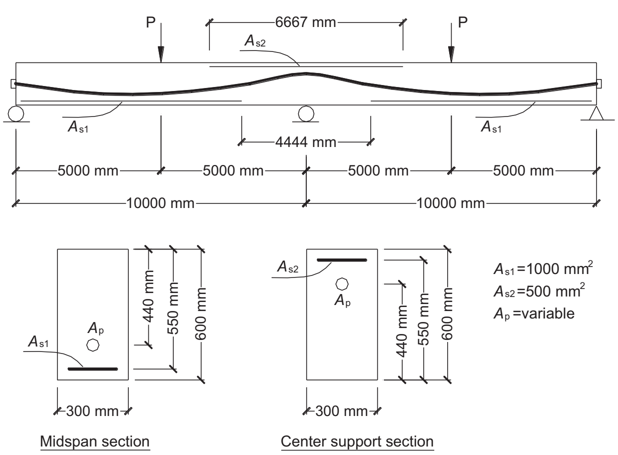

Fig. 5. Details of continuous prestressed concrete beam for numerical evaluation.

Table 1
Material properties of FRP and steel tendons.

Tendons	Tensile strength (MPa)	Elastic modulus (GPa)	Ultimate strain (%)
AFRP	1500	68	2.2
CFRP	1840	147	1.25
Steel	1860	195	>3.5

Table 2
Normalized ultimate tendon stress and concrete strains as well as failure mode of the beams.

Tendons	ω_p	σ_p/f_{pu}	σ_p/f_f	$\varepsilon_{c1}/\varepsilon_u$	$\varepsilon_{c2}/\varepsilon_u$	Failure mode
AFRP	0.024	–	1.0	0.56	0.62	Rupture
	0.048	–	1.0	0.68	0.72	Rupture
	0.084	–	1.0	0.85	0.87	Rupture
	0.108	–	0.99	1.0	0.97	Crushing Approx. rupture
CFRP	0.144	–	0.91	1.0	0.99	Crushing
	0.204	–	0.83	1.0	0.99	Crushing
	0.024	–	1.0	0.45	0.51	Rupture
	0.048	–	1.0	0.6	0.63	Rupture
	0.084	–	1.0	0.84	0.82	Rupture
	0.108	–	0.98	1.0	0.98	Crushing Approx. rupture
Steel	0.144	–	0.89	1.0	0.98	Crushing
	0.204	–	0.77	1.0	1.0	Crushing
	0.024	0.97	–	1.0	0.89	Crushing
	0.048	0.96	–	1.0	0.89	Crushing
	0.084	0.95	–	1.0	0.92	Crushing
	0.108	0.93	–	1.0	0.97	Crushing
	0.144	0.89	–	1.0	0.98	Crushing
	0.204	0.78	–	1.0	1.0	Crushing

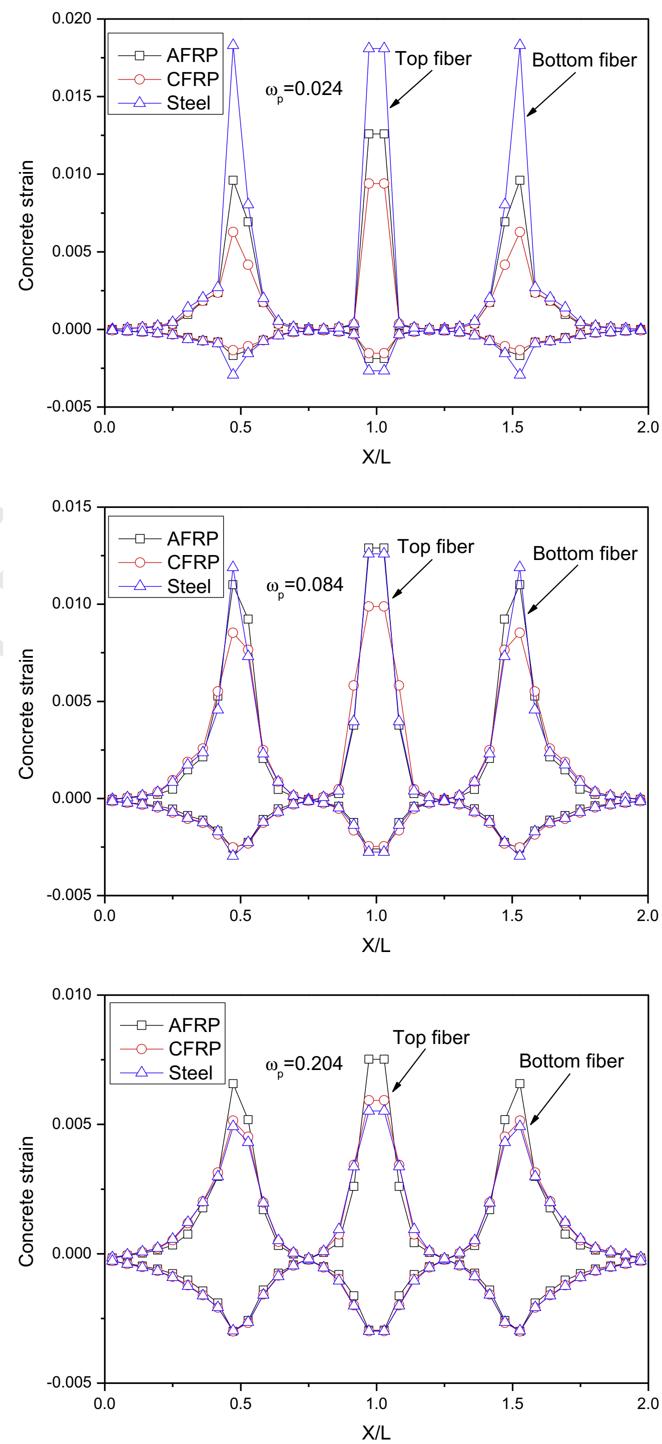

Fig. 6. Concrete strain distribution over the length for different tendon types and various ω_p levels.

Please cite this article in press as: Lou T et al. A comparative study of continuous beams prestressed with bonded FRP and steel tendons. Compos Struct (2015), http://dx.doi.org/10.1016/j.compstruct.2015.01.009

The prestressing steel used in the present numerical investigation is assumed to be Grade 270, 7-wire low relaxation strands and the values of K, Q and R are 1.0618, 0.01174 and 7.344, respectively. The prestressing FRP tendons are linear elastic up to rupture, as shown in Fig. 1(c).

The nonprestressed steel is assumed to be linear elastic prior to yielding and perfectly plastic after yielding, as shown in Fig. 1(d).

2.2. Finite element model

A finite element model based on the Euler–Bernoulli beam theory has been developed. The model is an extension of a previously developed model for unbonded prestressed concrete continuous beams [24], in which the contribution of unbonded tendons was not included in the stiffness matrix but was made by transforming the prestressing force into equivalent nodal loads. For analysis of bonded prestressed concrete beams, however, the contribution of bonded tendons to the stiffness matrix must be considered because of the compatibility of strains between prestressing tendons and the surrounding concrete.

Consider a two-node plane beam element to be described in the local coordinate system (x, y), as shown in Fig. 2. The node points are assumed to be at the centroid of the cross-sections. The prestressing tendon segment in the beam element is idealized to be

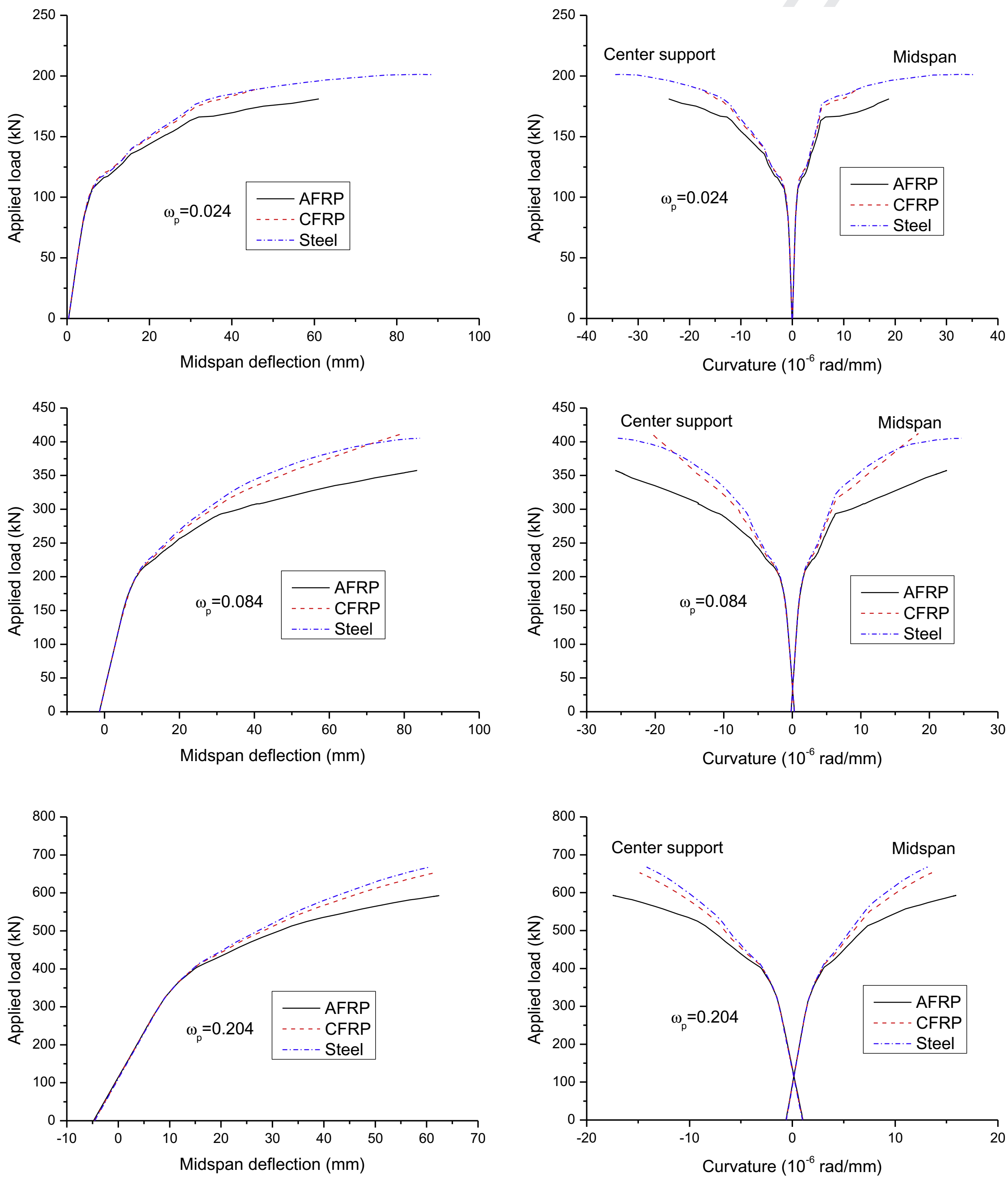

(a) (b)

Fig. 7. Load-deformation response for different tendon types and various ω_p levels. (a) Load–deflection response; (b) load-curvature response.

Please cite this article in press as: Lou T et al. A comparative study of continuous beams prestressed with bonded FRP and steel tendons. Compos Struct (2015), http://dx.doi.org/10.1016/j.compstruct.2015.01.009

parallel with the centroidal axis, with eccentricity equal to the mean value of the eccentricities at the end nodes. Each node has three degrees of freedom: axial displacement u, transverse displacement v, and rotation θ. Assuming that u and v are a linear function and a cubic polynomial of x, respectively, they can be expressed in terms of element nodal displacements as follows:

$$u = (1-\xi)u_1 + \xi u_2 \tag{1a}$$

$$v = \left(1-3\xi^2+2\xi^3\right)v_1 + l\xi(1-\xi)^2\theta_1 + \left(3\xi^2-2\xi^3\right)v_2 + l\left(-\xi^2+\xi^3\right)\theta_2 \tag{1b}$$

where l = length of the beam element; and $\xi = x/l$.

The axial strain ε_0 on any point of the beam element is given by:

$$\varepsilon_0 = \frac{\partial u}{\partial x} + \frac{1}{2}\left(\frac{\partial v}{\partial x}\right)^2 \tag{2}$$

The second term of the right side of the above equation represents the large displacement effects. Assuming that the shear deformation of the element is negligible, which is a reasonable approximation for slender (Euler–Bernoulli) beams commonly used for prestressing applications, the section curvature ϕ is expressed by

$$\phi = -\frac{\partial^2 v}{\partial x^2} \tag{3}$$

Assuming that a plane section remains plane during bending and that perfect bond exists between the reinforcement and the surrounding concrete, the strain ε at any fiber of the section is given by:

$$\varepsilon = \varepsilon_0 + y\phi \tag{4}$$

The element nodal displacement vector $\boldsymbol{u}^e$ and element nodal force vector $\boldsymbol{P}^e$ may be written as

$$\boldsymbol{u}^e = \{u_1 \quad v_1 \quad \theta_1 \quad u_2 \quad v_2 \quad \theta_2\}^T \tag{5}$$

$$\boldsymbol{P}^e = \{N_1 \quad V_1 \quad M_1 \quad N_2 \quad V_2 \quad M_2\}^T \tag{6}$$

According to the total Lagrangian description, the tangent stiffness equations for an element can be determined by applying the principle of virtual work as follows:

$$d\boldsymbol{P}^e = \boldsymbol{K}_t^e d\boldsymbol{u}^e = (\boldsymbol{K}_1^e + \boldsymbol{K}_2^e + \boldsymbol{K}_3^e)d\boldsymbol{u}^e \tag{7}$$

$$\boldsymbol{K}_1^e = \int_l \boldsymbol{B}_l^T \boldsymbol{D}_t \boldsymbol{B}_l dx \tag{8a}$$

$$\boldsymbol{K}_2^e = \int_l \boldsymbol{B}_l^T \boldsymbol{D}_t \boldsymbol{B}_n dx + \int_l \boldsymbol{B}_n^T \boldsymbol{D}_t \boldsymbol{B}_l dx + \int_l \boldsymbol{B}_n^T \boldsymbol{D}_t \boldsymbol{B}_n dx \tag{8b}$$

$$\boldsymbol{K}_3^e = \int_l N \boldsymbol{J}^T \boldsymbol{J} dx \tag{8c}$$

$$\boldsymbol{B}_l = \begin{bmatrix} -\frac{1}{l} & 0 & 0 & \frac{1}{l} & 0 & 0 \\ 0 & \frac{6}{l^2} - \frac{12\xi}{l^2} & \frac{4}{l} - \frac{6\xi}{l} & 0 & -\frac{6}{l^2} + \frac{12\xi}{l^2} & \frac{2}{l} - \frac{6\xi}{l} \end{bmatrix} \tag{9a}$$

$$\boldsymbol{B}_n = [1 \quad 0]^T \boldsymbol{u}^{eT} \boldsymbol{J}^T \boldsymbol{J} \tag{9b}$$

$$\boldsymbol{J} = \begin{bmatrix} 0 & -\frac{6\xi}{l} + \frac{6\xi^2}{l} & 1 - 4\xi + 3\xi^2 & 0 & \frac{6\xi}{l} - \frac{6\xi^2}{l} & -2\xi + 3\xi^2 \end{bmatrix} \tag{10}$$

$$\boldsymbol{D}_t = \begin{bmatrix} d_{11} & d_{12} \\ d_{21} & d_{22} \end{bmatrix} \tag{11}$$

$$d_{11} = \sum_i E_{tci}A_{ci} + \sum_j E_{tsj}A_{sj} + \sum_k E_{tpk}A_{pk} \tag{12a}$$

$$d_{12} = d_{21} = \sum_i E_{tci}A_{ci}y_{ci} + \sum_j E_{tsj}A_{sj}y_{sj} + \sum_k E_{tpk}A_{pk}y_{pk} \tag{12b}$$

$$d_{22} = \sum_i E_{tci}A_{ci}y_{ci}^2 + \sum_j E_{tsj}A_{sj}y_{sj}^2 + \sum_k E_{tpk}A_{pk}y_{pk}^2 \tag{12c}$$

$$N = \sum_i \sigma_{ci}A_{ci} + \sum_j \sigma_{sj}A_{sj} + \sum_k \sigma_{pk}A_{pk} \tag{13}$$

where the summation symbol signifies that the cross section is divided into layers to employ a layered approach; the subscripts ci, sj and pk represent the ith concrete layer, jth nonprestressed steel layer and kth tendon layer, respectively; E_t is the tangent modulus for materials; A corresponds to the area and σ corresponds to the stress.

After assembling the equilibrium equations for the structure in the global coordinate system and imposing an appropriate boundary condition, a load or displacement control incremental method in combination with the Newton–Raphson iterative algorithm is used for the solution of the nonlinear equilibrium equations. During the solution process, when any of the constituent materials reaches its ultimate strain or strength capacity, failure is assumed to take place and the analysis is therefore terminated. The proposed model is capable of conducting the geometric and material nonlinear analysis of continuous concrete beams prestressed with bonded steel and FRP tendons over the entire loading range up to the ultimate. Time-dependent effects such as tendon relaxation and concrete creep are not covered in the present study, but the modeling of these effects may be seen elsewhere [25].

3. Verification of the proposed model

In order to validate the proposed nonlinear model, two of the continuous prestressed concrete beams tested by Lin [26] have been analyzed. These beams were designated as Beams A and B, and were tested under static loads up to failure. The structure and section details of the specimens are shown in Fig. 3. The beams were designed to be identical except for the content of nonprestressed steel: Beam B contained two 14 mm tensile steel bars over the midspan and center support regions while Beam A did not. The beams had a rectangular section (203.2 × 406.4 mm), and were 15392.4 mm long with two equal spans to which two concentrated loads were applied at 2621.3 mm from the center support. The tendon profile, which was designed to be concordant, was curved over the center support region and straight over other regions. The tendon consisted of 32 parallel 5 mm high-strength steel wires. The

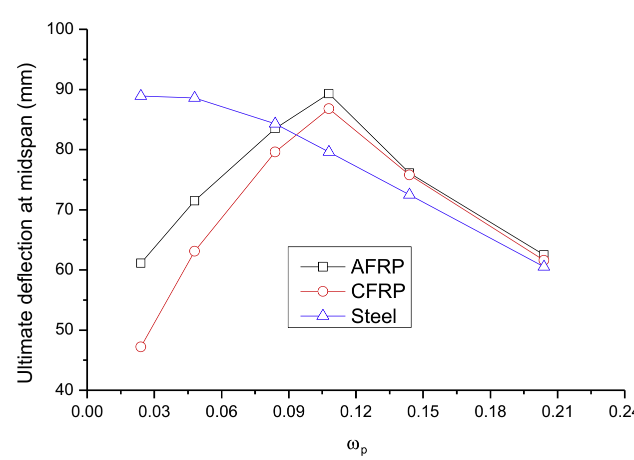

Fig. 8. Variation of ultimate deflection with ω_p level for different tendon types.

Please cite this article in press as: Lou T et al. A comparative study of continuous beams prestressed with bonded FRP and steel tendons. Compos Struct (2015), http://dx.doi.org/10.1016/j.compstruct.2015.01.009

ultimate tensile strength, yield stress and elastic modulus of the prestressing tendon were 1765, 1572 MPa and 200 GPa, respectively. The yield strength and elastic modulus of nonprestressed steel were 314 MPa and 196 GPa, respectively. The cylinder compressive strengths of concrete at age of 28 days were 36.2 MPa for Beam A and 41.3 MPa for Beam B. The tendon was tensioned to have an initial prestress of 979 MPa when the beams were 14 days old. About two weeks later the beams were loaded up to collapse.

Fig. 4 shows a comparison between experimental and computational results regarding the load versus moment responses at the center support and load point for the two test beams. The experimentally obtained moments were calculated according to the experimental values of the reaction at the end support reported in the literature. It can be seen in the graphs that proposed analysis reproduces with remarkable accuracy the moment evolution in both of the continuous prestressed concrete beams throughout the loading history up to failure.

4. Numerical investigation

A bonded prestressed concrete rectangular beam continuous over two equal spans to which two centre-point loads are symmetrically applied, as shown in Fig. 5, is used as a control beam for the

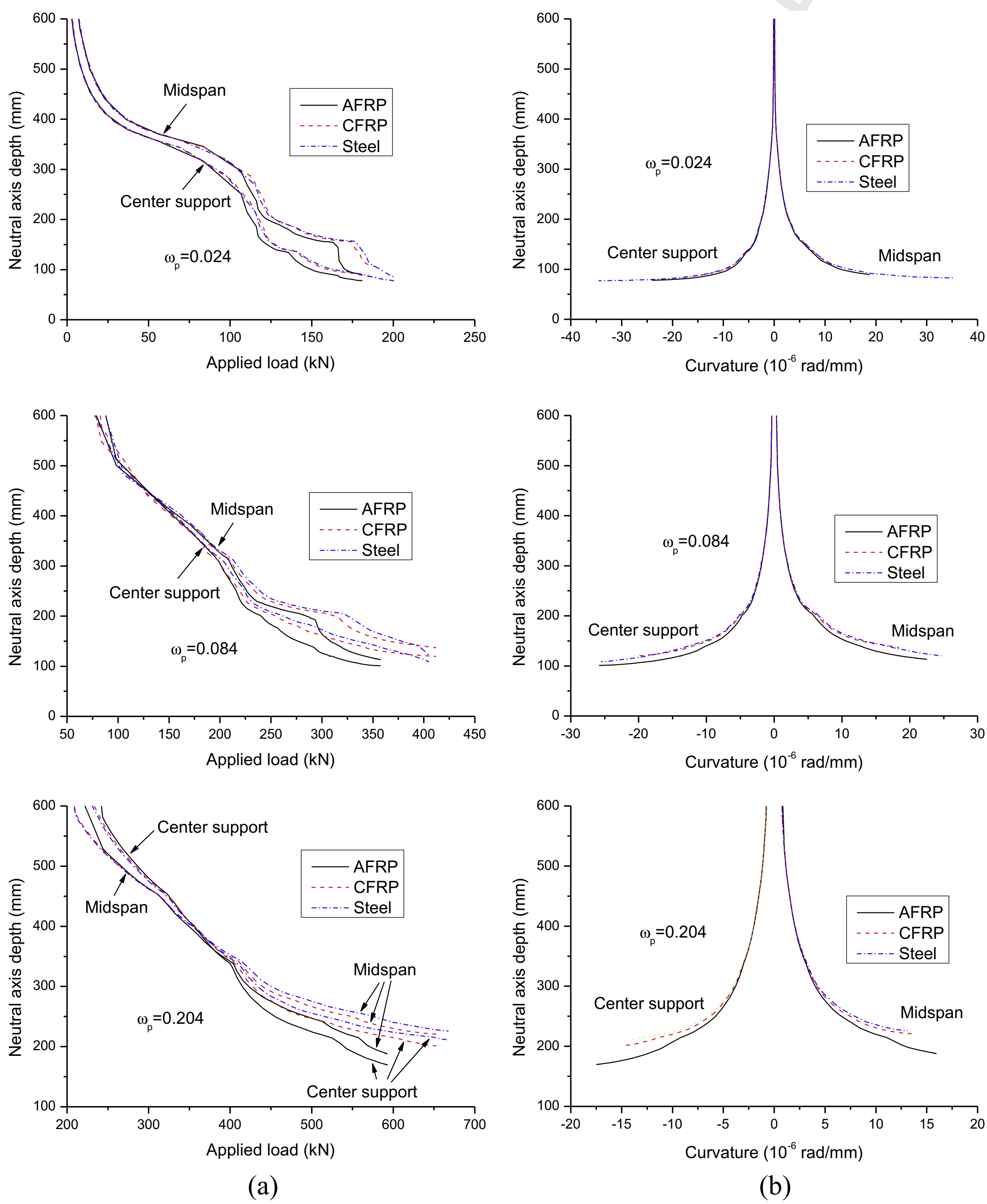

Fig. 9. Development of neutral axis depth for different tendon types and various ω_p levels. (a) Load versus neutral axis depth; (b) curvature versus neutral axis depth.

Please cite this article in press as: Lou T et al. A comparative study of continuous beams prestressed with bonded FRP and steel tendons. Compos Struct (2015), http://dx.doi.org/10.1016/j.compstruct.2015.01.009

numerical evaluation. The prestressing tendons are assumed to have an idealized parabolic profile with eccentricities at the end support, midspan and center support of 0, 140 and 140 mm, respectively. The beam contains nonprestressed tensile steel over the positive moment region ($A_{s1} = 1000\ \text{mm}^2$) and negative moment region ($A_{s2} = 500\ \text{mm}^2$). The yield strength and elastic modulus of nonprestressed steel are 450 MPa and 200 GPa, respectively. The concrete characteristic cylinder compressive strength f_{ck} (note: $f_{ck} = f_{cm} - 8$) is taken as 60 MPa. Three types of prestressing tendons are used: AFRP, CFRP and steel tendons. The material properties (tensile strength, elastic modulus and ultimate strain) for each type of tendons are summarized in Table 1. The yield stress of prestressing steel is taken as 90% of the tensile strength. The initial prestress f_{p0} is taken as 950 MPa. Various tendon areas A_p are used so as to generate various levels of reinforcement index of prestressing tendons ω_p, which is defined as

$$\omega_p = \frac{A_p f_{p0}}{b d_p f_{ck}} \tag{14}$$

where b is the section width and d_p is the effective depth of prestressing tendons at the center support or midspan. In this study, the ω_p level ranges from a minimum of 0.024 to a maximum of 0.204. In the finite element idealization, the concrete beam is divided into 36 two-node beam elements (18 elements for each span) with length of 555.56 mm each. Each element is subdivided into 10 concrete layers, 1 tendon layer and 1 nonprestressed steel layer.

4.1. Failure mode and crack pattern

A summary of the normalized tendon stress (σ_p/f_{pu} or σ_p/f_f) and concrete strains ($\varepsilon_{c1}/\varepsilon_u$ and $\varepsilon_{c2}/\varepsilon_u$) at failure as well as the failure mode of the beams is given in Table 2, where σ_p is the ultimate stress in tendons; f_{pu} and f_f are the tensile strengths of steel and FRP tendons, respectively; ε_{c1} and ε_{c2} are the concrete strains at ultimate in extreme compressive fiber of the midspan and center support sections, respectively. A normalized ultimate tendon stress of 1.0 indicates a rupture failure while a normalized ultimate concrete strain of 1.0 signifies a crushing failure. According to the present numerical tests, all the steel prestressed concrete beams have failed due to crushing of concrete at the critical section. At the lowest ω_p level of 0.024, failure of the steel prestressed beam takes place at midspan while at failure the center support section is still far below its ultimate strain capacity. As ω_p increases, the exploitation of the center support is enhanced. At the highest ω_p level of 0.204, the concrete is crushed both at midspan and at the center support. For FRP prestressed concrete beams, on the other hand, failure may take place either due to concrete crushing or tendon rupture, depending on the ω_p level. According to the present analysis, the tendon rupture and concrete crushing take place simultaneously when ω_p reaches around 0.108. A rupture failure appears for ω_p lower than 0.108 while a crushing failure occurs for ω_p higher than 0.108. At a low ω_p level (e.g., 0.024), the critical sections of a FRP prestressed concrete beam are far below their ultimate capacities when the tendons are ruptured. At a high ω_p level (e.g., 0.204), on the other hand, the FRP tendons are far below their ultimate tensile strength when the concrete is crushed.

At the failure loads, the concrete strain distribution over the length for different tendon types and various ω_p levels is displayed in Fig. 6, where X/L is the ratio of the distance from the end support to the span. From the graphs in this figure the crack pattern may be deduced. At ω_p of 0.024, the steel prestressed concrete beam develops very large tensile strains in the critical positive and negative moment regions, while the tensile strains over other regions are small. This observation indicates that there are a few main cracks with large widths in the critical regions while the cracks in other regions are insignificant. In other words, there appears crack concentration in the beam containing a low amount of steel reinforcement. As ω_p increases, the crack pattern of the steel prestressed concrete beam appears to be improved, that is, the maximum crack widths are reduced and the crack zones are extended. The crack pattern for FRP prestressed concrete beams is related to the failure mode. At a low ω_p level (e.g., 0.024), failure is caused by rupture of FRP tendons and, therefore, crack concentration is not as important as the case of the steel prestressed concrete beam. At a high ω_p level (e.g., 0.204), crushing failure happens. In this case, the crack pattern of the CFRP prestressed concrete beam is very similar to that of the steel prestressed concrete beam, while the AFRP prestressed concrete beam develops obviously bigger crack widths at the critical regions than the CFRP or steel prestressed concrete beam.

4.2. Deformation characteristics

Prior to the application of external loads, there are initial deformations as a result of combined prestressing and self-weight. At the lowest ω_p level of 0.024, the self-weigh effect prevails over the prestressing effect, thereby resulting in a downward deflection of the beam as well as a sagging curvature at midspan and a hogging curvature at the center support. For ω_p greater than 0.048, the prestressing effect overrides the self-weight effect, causing a camber of the beam as well as a hogging curvature at midspan and a sagging curvature at the center support. The entire load–deflection and load-curvature responses for different tendon types and various ω_p levels are shown in Fig. 7(a) and (b), respectively. Before cracking, the behavior is primarily controlled by concrete and, therefore, the responses for different tendon types are almost identical. After cracking, the contribution of prestressing reinforcement is increasingly important. Due to lower modulus of elasticity, AFRP tendons mobilize smaller bending stiffness of a beam than CFRP or steel tendons. At a high ω_p level (in the case of crushing failure), the entire load-deformation response characteristics of the CFRP prestressed beam are similar to those of the steel prestressed beam. However, at a low ω_p level, the load-deformation behavior of FRP prestressed beams may be undesirable because of premature failure caused by tendon rupture.

Fig. 8 shows the variation of ultimate deflection with the ω_p level for different tendon types. At the lowest ω_p level of 0.024, the ultimate deflections of AFRP and CFRP prestressed beams are respectively 31.3% and 46.9% lower than that of the steel prestressed beam. As ω_p increases, the ultimate deflection for steel tendons gradually decreases while the ultimate deflections for

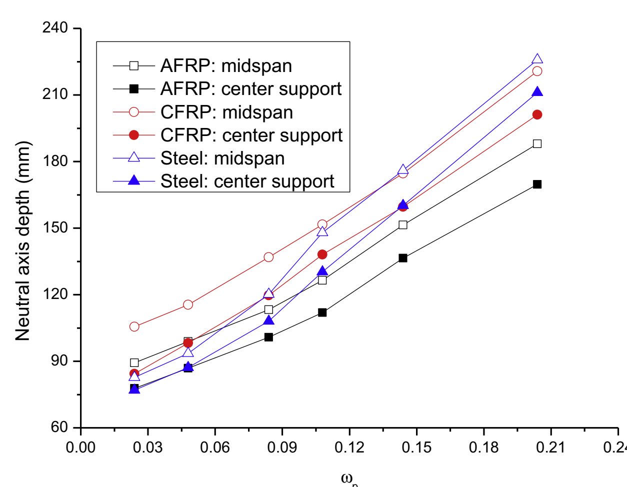

Fig. 10. Variation of neutral axis depth with ω_p level for different tendon types.

Please cite this article in press as: Lou T et al. A comparative study of continuous beams prestressed with bonded FRP and steel tendons. Compos Struct (2015), http://dx.doi.org/10.1016/j.compstruct.2015.01.009

FRP tendons increase quickly. When ω_p reaches 0.108 (transition from a rupture failure to a crushing failure), the deflections for FRP tendons turn to be obviously higher than that for steel tendons. With the continuing increase of ω_p, the deflections for both steel and FRP tendons decrease, but the decrease in deflection for steel tendons tends to be slower than those for FRP tendons. At the highest ω_p level of 0.204, the discrepancy between the deflections for steel and FRP tendons appears to be insignificant. At a low level of ω_p, the deflection for CFRP tendons is smaller than that for AFRP tendons, but the difference gradually diminishes with the increase of ω_p, and appears to be not noticeable as ω_p increases to 0.144 or above.

4.3. Neutral axis depth

The initial neutral axis depth for a prestressed concrete beam under prestressing and self-weight may be positive or negative, depending on the ω_p level. At ω_p of 0.024, the initial neutral axis depths are about 900 mm at midspan and 680 mm at the center support, that is, the neutral axis is initially located below the bottom fiber of the midspan section and above the top fiber of the center support section. At ω_p of 0.204, the initial neutral axis depths are about −50 mm at midspan and 90 mm at the center support, that is, the neutral axis is initially located outside the midspan section (above the top fiber) while inside the center support section.

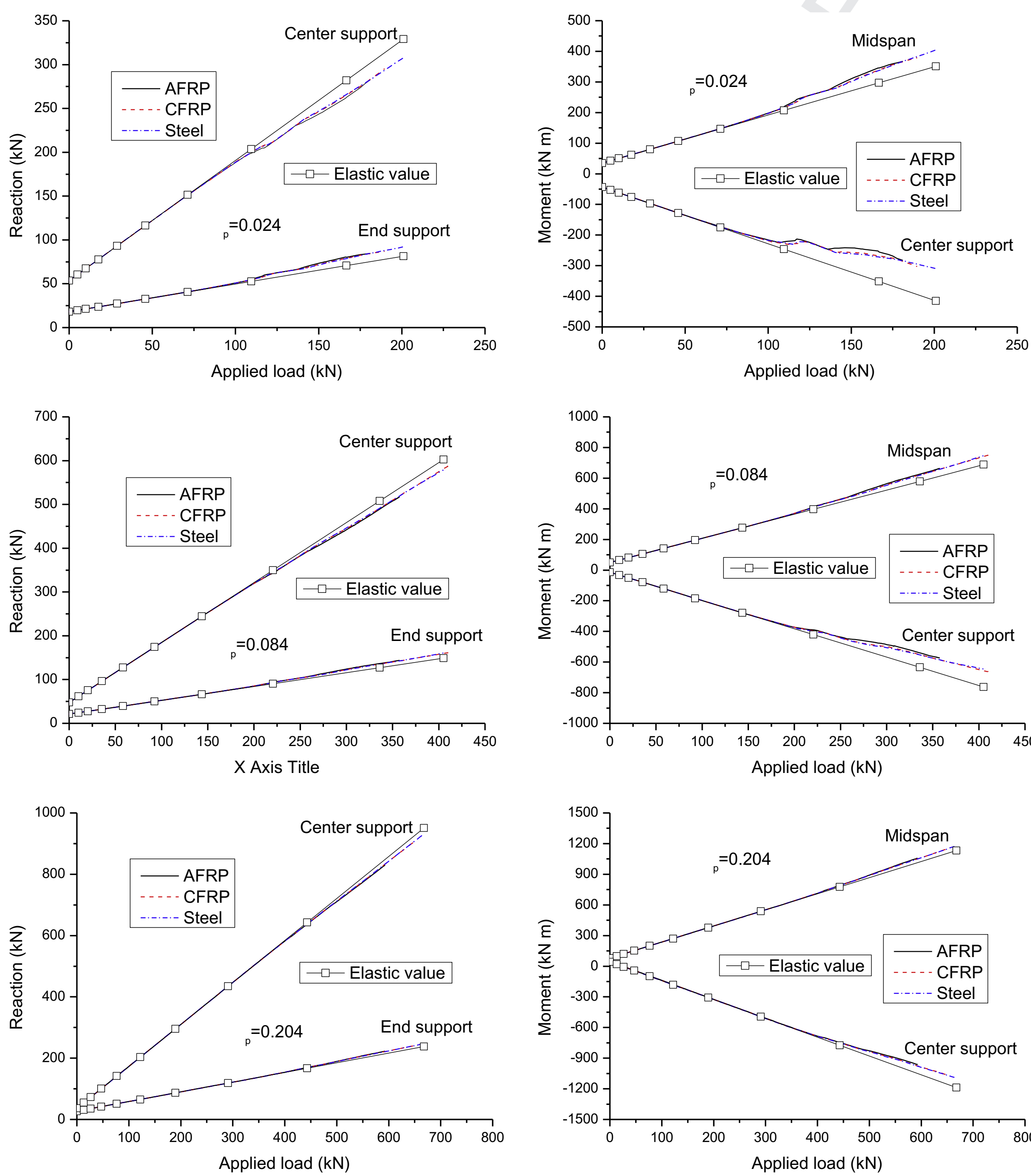

(a) (b)

Fig. 11. Development of support reaction and bending moment for different tendon types and various ω_p levels. (a) Load-reaction response; (b) load-moment response.

The neutral axis moves rapidly as the external loads are applied and gradually increased.

The evolution of neutral axis depth with the applied load and curvature, after the neutral axis reaches the extreme tension fiber of the section, for different tendon types and various ω_p levels is shown in Fig. 9(a) and (b), respectively. It is seen in Fig. 9(a) that at a low ω_p level, the development of neutral axis depth exhibits a significantly nonlinear manner and the neutral axes at the center support and midspan move at almost the same rate. As ω_p increases, the nonlinear manner is obviously reduced and the movement of neutral axis at the center support may become faster than that at midspan. After the evolution of cracks stabilizes, the shift of neutral axis in the AFRP prestressed concrete beam appears to be faster than that in the CFRP or steel prestressed concrete beam. From Fig. 9(b) it is seen that the neutral axis moves rapidly at first but the movement tends to slow down as the hogging or sagging curvature increases. After stabilizing of the crack development, at a given curvature, AFRP tendons mobilizes lower neutral axis depth than CFRP or steel tendons, particularly obvious at a high ω_p level.

Fig. 10 shows the variation of neutral axis depth at ultimate with the ω_p level for different tendon types. It is seen that the neutral axis depth increases as ω_p increases. The rate of increase in neutral axis depth for steel tendons tends to be faster than that for FPP tendons. At a given ω_p level, the midspan section develops higher neutral axis depth than the center support section. AFRP tendons mobilize lower neutral axis depth at the midspan or center support section than CFRP tendons. At a low ω_p level, the neutral axis depth for steel tendons is close to that for AFRP tendons, while at a high ω_p level the neutral axis depths for steel and CFRP tendons are comparable.

4.4. Development of support reaction and bending moment

The development of reactions at the end and center supports for different tendon types and various ω_p levels is illustrated in Fig. 11(a), while the evolution of bending moments at the midspan and center support is shown in Fig. 11(b). The elastic values, calculated based on the linear-elastic theory, are also displayed in the graphs. The secondary reactions and moments due to prestressing are included in the values shown in these graphs. The magnitude and direction of secondary reactions and moments are dependent on the layout of tendons. For the beams analyzed in this study, the tendon line is below its linearly transformed concordant line. As a result, the secondary reaction at the end support is positive but negative at the center support, causing positive secondary moments in the beams.

It can be seen in Fig. 11 that at initial loading, the actual reaction and moment develop linearly with the applied load, indicating there is no redistribution of moments in this elastic stage. After cracking, the actual values appear to deviate from the elastic ones due to redistribution of moments. Because cracking appears firstly at the center support, upon cracking the moments tend to be redistributed from the center support zone towards the midspan zone. As a consequence, there is a diminution of the rate of increase in reaction and moment at the center support and, correspondingly, a growth of the rate of increase in end support reaction and midspan moment. In the inelastic ranges, the deviation of the actual reaction and moment from the elastic values is notable at a low ω_p level but tends to diminish as ω_p increases, as can be observed in Fig. 11.

4.5. Degree of moment redistribution

Fig. 12 shows the development of the degree of moment redistribution for different tendon types and various ω_p levels. The degree of moment redistribution β is defined by: $\beta = 1 - (M/M_e)$, where M and M_e are the actual and elastic moments corresponding to a load level, respectively. The degree of moment redistribution is equal to zero until cracking. After cracking, the redistribution of moments takes place. The redistribution is positive at the center support while negative at midspan. At low and medium ω_p levels, the evolution of redistribution after cracking is obviously affected by several typical phases, namely, the stabilization of crack devel-

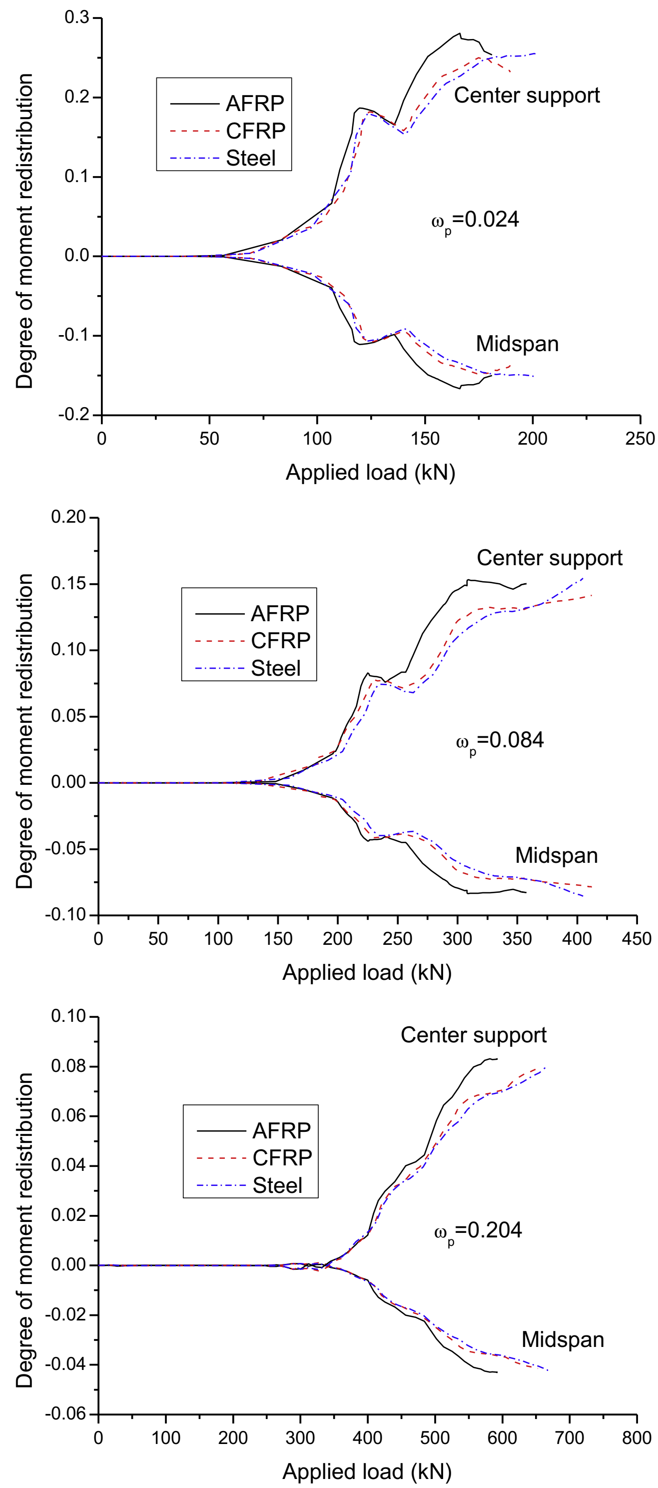

Fig. 12. Development of the degree of moment redistribution for different tendon types and various ω_p levels.

Please cite this article in press as: Lou T et al. A comparative study of continuous beams prestressed with bonded FRP and steel tendons. Compos Struct (2015), http://dx.doi.org/10.1016/j.compstruct.2015.01.009

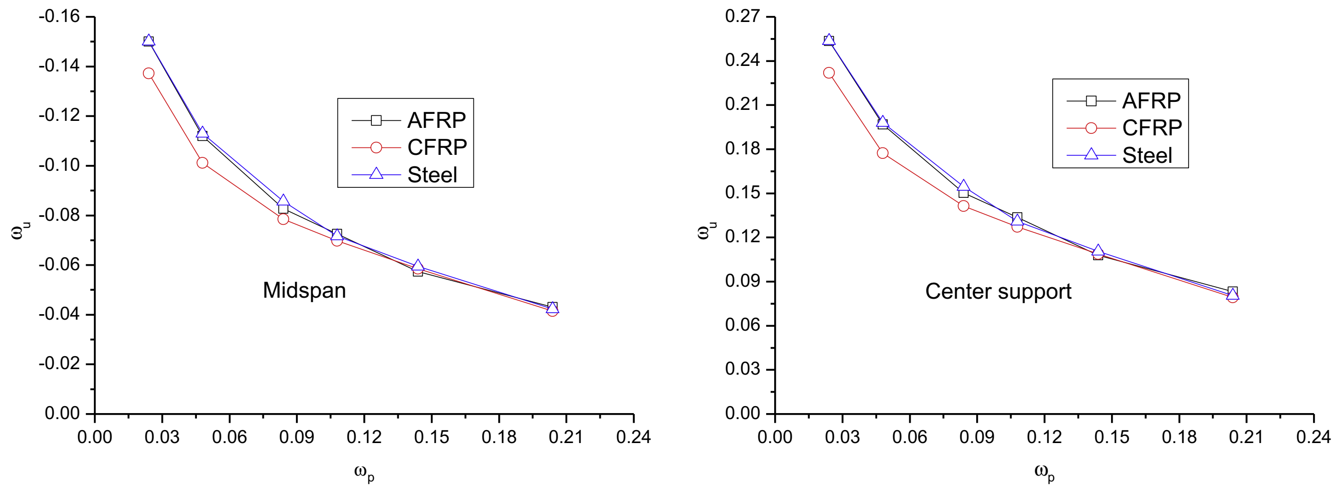

Fig. 13. Variation of the β_u value with ω_p level for different tendon types.

opment, yielding of nonprestressed steel at the center support and yielding of nonprestressed steel at midspan. At a high ω_p level, on the other hand, the influence of these phases on the redistribution development appears to be not so noticeable. For steel tendons, the maximum redistribution occurs at the ultimate limit state irrespective of the ω_p level. For FRP tendons, on the other hand, the maximum redistribution may not take place at failure at a low ω_p level.

Fig. 13 shows the variation of β_u (degree of moment redistribution at ultimate) with the ω_p level for different tendon types. It is seen that the β_u value decreases as ω_p increases. At a given ω_p level, the β_u values for AFRP and steel tendons are almost identical. The redistribution for CFRP tendons is obviously lower than that for steel tendons at a low ω_p level, but the difference between the β_u values for CFRP and steel tendons becomes negligible when ω_p is greater than 0.108.

5. Summary and conclusions

A numerical investigation has been carried out to reveal the flexural behavior of continuous concrete beams prestressed with bonded FRP and steel tendons. A finite element model based on the layered Euler–Bernoulli beam theory for full-range nonlinear analysis of continuous FRP and steel prestressed concrete beams has been developed. The model is validated against the experimental results. A comparative study is conducted on two-span continuous prestressed concrete beams with bonded AFRP, CFRP and steel tendons using the proposed model. A wide range of ω_p is used. Typical aspects of behavior of the beams are examined, including the failure mode and crack pattern, deformation characteristics, neutral axis depth and moment redistribution. Based on the results obtained from the analysis, the follow conclusions may be drawn:

- Failure of steel prestressed concrete beams is always attributed to crushing of concrete. On the other hand, FRP prestressed concrete beams may fail due to crushing of concrete or rupture of FRP tendons, depending on the ω_p level: when ω_p reaches around 0.108, concrete crushing and tendon rupture take place simultaneously; a rupture failure happens for ω_p lower than 0.108 while a crushing failure occurs for ω_p greater than 0.108.
- At a low reinforcement index, crack concentration appears in the steel prestressed concrete beam while this phenomenon is not so important in FRP prestressed concrete beams. At a high reinforcement index, AFRP tendons mobilize larger crack width than CFRP and steel tendons.
- At a low ω_p level, the ultimate deflection for FRP tendons is significantly lower than that for steel tendons. As ω_p increases, the ultimate deflection for steel tendons consistently decreases while the deflection for FRP tendons quickly increases up to ω_p of 0.108 and then turns to decrease. The deflection difference between FRP and steel tendons appears to be insignificant at a high ω_p level.
- Due to a lower modulus of elasticity, AFRP tendons register lower neutral axis depth at ultimate than CFRP tendons. At a low ω_p level, the neutral axis depth mobilized by steel tendons is close to that mobilized by AFRP tendons while, at a high ω_p level, it is close to that mobilized by CFRP tendons.
- The maximum redistribution of moments in steel prestressed concrete beams takes place at ultimate, but this may not true for FRP prestressed concrete beams. At a given ω_p level, the redistribution at ultimate for AFRP tendons is almost identical to that for steel tendons. At a low ω_p level, CFRP tendons mobilize obviously lower moment redistribution than steel tendons but the redistribution difference between CFRP and steel tendons is negligible at a high ω_p level.

Acknowledgments

This research is sponsored by FEDER funds through the program COMPETE (Programa Operacional Factores de Competitividade) and by national funds through FCT (Fundação para a Ciência e a Tecnologia) under the project PEst-C/EME/UI0285/2013. The work presented in this paper has also been supported by FCT under Grant No. SFRH/BPD/66453/2009.

References

[1] De Domenico D, Pisano AA, Fuschi P. A FE-based limit analysis approach for concrete elements reinforced with FRP bars. Compos Struct 2014;107:594–603.
[2] Mahroug MEM, Ashour AF, Lam D. Experimental response and code modelling of continuous concrete slabs reinforced with BFRP bars. Compos Struct 2014;107:664–74.
[3] Ferreira D, Oller E, Barris C, Torres L. Shear strain influence in the service response of FRP reinforced concrete beams. Compos Struct 2015;121:142–53.
[4] Zaman A, Gutub SA, Wafa MA. A review on FRP composites applications and durability concerns in the construction sector. J Reinf Plast Compos 2013;32(24):1966–88.
[5] Schmidt JW, Bennitz A, Taljsten B, Goltermann P, Pedersen H. Mechanical anchorage of FRP tendons – a literature review. Constr Build Mater 2012;32:110–21.
[6] Elrefai A, West JS, Soudki K. Performance of CFRP tendon-anchor assembly under fatigue loading. Compos Struct 2007;80:352–60.
[7] Li F, Zhao QL, Chen HS, Wang JQ, Duan JH. Prediction of tensile capacity based on cohesive zone model for bond anchorage for fiber-reinforced polymer tendon. Compos Struct 2010;92:2400–5.

Please cite this article in press as: Lou T et al. A comparative study of continuous beams prestressed with bonded FRP and steel tendons. Compos Struct (2015), http://dx.doi.org/10.1016/j.compstruct.2015.01.009

[8] Fang Z, Zhang K, Tu B. Experimental investigation of a bond-type anchorage system for multiple FRP tendons. Eng Struct 2013;57:364–73.
[9] Puigvert F, Crocombe AD, Gil L. Static analysis of adhesively bonded anchorages for CFRP tendons. Constr Build Mater 2014;61:206–15.
[10] Puigvert F, Gil L, Escrig C, Bernat E. Stress relaxation analysis of adhesively bonded anchorages for CFRP tendons. Constr Build Mater 2014;66:313–22.
[11] ACI Committee 440. Guide for the design and construction of externally bonded FRP systems for strengthening concrete structures. ACI 440.2R-08, American Concrete Institute, Farmington Hills, MI; 2008.
[12] FIB. Model Code 2010. Bulletins 55 and 56, International Federation for Structural Concrete, Lausanne, Switzerland; 2012.
[13] Pisani MA. A numerical survey on the behaviour of beams pre-stressed with FRP cables. Constr Build Mater 1998;12:221–32.
[14] Park SY, Naaman AE. Shear behavior of concrete beams prestressed with FRP tendons. PCI J 1999;44(1):74–85.
[15] Toutanji H, Saafi M. Performance of concrete beams prestressed with aramid fiber-reinforced polymer tendons. Compos Struct 1999;44:63–70.
[16] Stoll F, Saliba JE, Casper LE. Experimental study of CFRP-prestressed high-strength concrete bridge beams. Compos Struct 2000;49:191–200.
[17] Dolan CW, Swanson D. Development of flexural capacity of a FRP prestressed beam with vertically distributed tendons. Compos Part B: Eng 2002;33:1–6.
[18] Kim YJ. Flexural response of concrete beams prestressed with AFRP tendons: numerical investigation. ASCE J Compos Constr 2010;14(6):647–58.
[19] Lou T, Lopes SMR, Lopes AV. Flexure of continuous HSC beams with external CFRP tendons: effects of fibre elastic modulus and steel ratio. Compos Struct 2014;116:29–37.
[20] Lou T, Lopes SMR, Lopes AV. External CFRP tendon members: secondary reactions and moment redistribution. Compos Part B: Eng 2014;57:250–61.
[21] Lou T, Lopes SMR, Lopes AV. Factors affecting moment redistribution at ultimate in continuous beams prestressed with external CFRP tendons. Compos Part B: Eng 2014;66:136–46.
[22] CEN. Eurocode 2: Design of concrete structures – Part 1–1: General rules and rules for buildings. EN 1992-1-1, European Committee for Standardization, Brussels, Belgium; 2004.
[23] Menegotto M, Pinto PE. Method of analysis for cyclically loaded reinforced concrete plane frames. IABSE preliminary report for symposium on resistance and ultimate deformability of structures acted on well-defined repeated loads, Lisbon; 1973. p. 15–22.
[24] Lou T, Lopes SMR, Lopes AV. Nonlinear and time-dependent analysis of continuous unbonded prestressed concrete beams. Comput Struct 2013;119:166–76.
[25] Lou T, Lopes SMR, Lopes AV. A finite element model to simulate long-term behavior of prestressed concrete girders. Finite Elem Anal Des 2014;81:48–56.
[26] Lin TY. Strength of continuous prestressed concrete beams under static and repeated loads. ACI J 1955;26(10):1037–59.

Please cite this article in press as: Lou T et al. A comparative study of continuous beams prestressed with bonded FRP and steel tendons. Compos Struct (2015), http://dx.doi.org/10.1016/j.compstruct.2015.01.009